Systematic investigation of emergent particles in type-III magnetic space groups

Gui-Bin Liu (刘贵斌) ⬤,[1,*] Zeying Zhang (张泽英),[2,*] Zhi-Ming Yu (余智明),[1] Shengyuan A. Yang (杨声远),[3]
and Yugui Yao (姚裕贵)[1,†]

[1]*Centre for Quantum Physics, Key Laboratory of Advanced Optoelectronic Quantum Architecture and Measurement (MOE),
School of Physics, Beijing Institute of Technology, Beijing 100081, China
and Beijing Key Laboratory of Nanophotonics and Ultrafine Optoelectronic Systems,
School of Physics, Beijing Institute of Technology, Beijing 100081, China*

[2]*College of Mathematics and Physics, Beijing University of Chemical Technology, Beijing 100029, China*

[3]*Research Laboratory for Quantum Materials, Singapore University of Technology and Design, Singapore 487372, Singapore*

In three-dimensional (3D) crystals, emergent particles arise when two or multiple bands contact and form degeneracy (band crossing) in the Brillouin zone. Recently a complete classification of emergent particles in 3D nonmagnetic crystals, described by the type-II magnetic space groups (MSGs), has been established. However, symmetries become complex in magnetically ordered structures. Consequently, we further perform a systematic investigation of emergent particles in magnetic crystals, and here we address this challenging task by exploring the possibilities of the emergent particles in the 674 type-III MSGs. Based on effective $\boldsymbol{k} \cdot \boldsymbol{p}$ Hamiltonian and our classification of emergent particles [Yu *et al.*, Sci. Bull. (2022)], we identify all possible emergent particles, including spinful and spinless, essential and accidental particles in the type-III MSGs. We find that all emergent particles in type-III MSGs also exist in type-II MSGs, with only one exception, i.e., the combined quadratic nodal line and nodal surface. Moreover, tabulations of the emergent particles in each of the 674 type-III MSGs, together with the symmetry operations, the small corepresentations, the effective $\boldsymbol{k} \cdot \boldsymbol{p}$ Hamiltonians, and the topological character of these particles, are explicitly presented. Remarkably, combining this work and our homemade `SpaceGroupIrep` and `MSGCorep` packages will provide an efficient way to search topological magnetic materials with novel quasiparticles.

I. INTRODUCTION

Since the discovery of topological Weyl and Dirac semimetals, the investigation of emergent particles has experienced rapid development and been attracting a variety of interests in condensed matter physics [1–23]. Compared with the elementary particles in high-energy physics, the quasiparticles in solids have much more abundant species due to looser symmetry constraints and then embrace more rich physics [24–37]. Thus identifying and classifying all the possible emergent particles in solids becomes a fundamentally important but also challenging work. Recently, in Ref. [38] we presented a complete list of emergent particles in three-dimensional (3D) nonmagnetic crystals with $\mathcal{T}$ symmetry. In this work, we establish such a list for the 3D magnetic crystals belonging to type-III magnetic space groups (MSGs).

In three dimensions, the crystal structure of materials is described by the symmetry of space groups (SGs). By introducing magnetic order, the crystals exhibit one more degree of freedom and then should be described by MSGs. There are in total 1651 MSGs which are divided into four types. The type-I MSGs are just the ordinary SGs, and do not have any antiunitary operation. In contrast, the general form of the other three types of MSGs can be written

$$M = S + \mathcal{A}S \tag{1}$$

with S a unitary subgroup with index 2 of the MSG M and $\mathcal{A}$ an antiunitary operation. M can be constructed from an ordinary SG G. When $S = G$, the MSGs can be further classified into two types by whether $\mathcal{A}$ is time reversal symmetry $\mathcal{T}$ (type II) or a combined operation of $\mathcal{T}$ and a pure translation (type IV). One then knows that the type-II MSGs have $\mathcal{T}$ symmetry and are applied to nonmagnetic crystals. In type-III MSGs, S is an isotranslational (translationengleiche) subgroup of G with index 2 and $\mathcal{A}$ is a combined operation containing $\mathcal{T}$ and a unitary (spatial) operation in $G - S$, making $\mathcal{A}S = \mathcal{T}(G - S)$.

It is clear that the symmetry of the type-III MSGs is lower than that of the type-II MSGs and heretofore most studies on emergent particles are in systems with $\mathcal{T}$ symmetry, i.e., the systems belonging to the type-II MSGs. However, it should be noted that the emergent particles also can appear in magnetic systems [1,39–44]. Actually, the original candidate for topological Weyl semimetal is a magnetic material [1]. In Ref. [39], Tang *et al.* predicted orthorhombic antiferromagnet CuMnAs as a candidate of magnetic Dirac semimetal. Moreover, novel emergent particles in magnetic materials with higher-order dispersion or 1D manifold of degeneracy also has been unveiled in previous works [45–47]. However, people still lack an overall and systematic understanding about what

TABLE I. Classification and statistics of emergent particles in type-III MSGs. Similar to Ref. [38], Abbr is the abbreviation for the notation of emergent particle, d_m is the dimension of the degeneracy manifold, d is the degree of degeneracy of the band crossing, Ld is the leading order of the band splitting near the crossing, and $\mathcal{C}$ is the topological charge (Chern number for nodal point or Berry phase for nodal line) of the emergent particles. N_{ess} (N_{acc}) is the spinless particle's occurrence number in SM Sec. III A (SM Sec. III B) for essential (accidental) degeneracy, and N_{ess}^{SOC} (N_{acc}^{SOC}) is similar but for spinful particles in SM Sec. III C (SM Sec. III D). The number in the parentheses is the number of MSGs that host the particle.

Notation	Abbr	d_m	d	Ld	$|\mathcal{C}|$	Occurrence number			
						N_{ess}	N_{acc}	N_{ess}^{SOC}	N_{acc}^{SOC}
Charge-1 Weyl point	C-1 WP	0	2	(111)	1	130 (59)	1448 (321)	218 (76)	1448 (321)
Charge-2 Weyl point	C-2 WP	0	2	(122)	2	83 (37)	228 (56)	29 (21)	228 (56)
Charge-3 Weyl point	C-3 WP	0	2	(133)	3	×	42 (14)	×	42 (14)
Charge-4 Weyl point	C-4 WP	0	2	(223)	4	×	×	×	×
Triple point	TP	0	3	(111)	–	47 (18)	748 (222)	×	67 (27)
Charge-2 triple point	C-2 TP	0	3	(111)	2	15 (10)	×	5 (5)	×
Quadratic triple point	QTP	0	3	(122)	–	×	28 (10)	×	×
Quadratic contact triple point	QCTP	0	3	(222)	0	60 (26)	×	×	×
Dirac point	DP	0	4	(111)	0	83 (59)	173 (102)	349 (161)	565 (236)
Charge-2 Dirac point	C-2 DP	0	4	(111)	2	2 (2)	30 (30)	6 (4)	30 (30)
Charge-4 Dirac point	C-4 DP	0	4	(111)	4	×	×	×	×
Quadratic Dirac point	QDP	0	4	(122)	0	42 (30)	18 (18)	9 (7)	10 (10)
Charge-4 quadratic Dirac point	C-4 QDP	0	4	(122)	4	×	×	×	×
Quadratic contact Dirac point	QCDP	0	4	(222)	0	×	×	13 (10)	×
Cubic Dirac point	CDP	0	4	(133)	0	×	×	1 (1)	×
Cubic crossing Dirac point	CCDP	0	4	(223)	0	3 (3)	×	×	×
Sextuple point	SP	0	6	(111)	0	8 (8)	×	4 (4)	×
Charge-4 sextuple point	C-4 SP	0	6	(111)	4	×	×	×	×
Quadratic contact sextuple point	QCSP	0	6	(222)	0	×	×	×	×
Octuple point	OP	0	8	(111)	0	×	×	3 (3)	×
Weyl nodal line	WNL	1	2	(11)	π	1510 (395)	3525 (470)	1243 (262)	1082 (232)
Weyl nodal line net	WNL net	1	2	(11)	π	1143 (274)	1222 (294)	685 (150)	148 (57)
Quadratic nodal line	QNL	1	2	(22)	0	740 (173)	×	61 (19)	×
Cubic nodal line	CNL	1	2	(33)	π	×	×	×	×
Dirac nodal line	DNL	1	4	(11)	0	12 (4)	×	223 (52)	178 (51)
Dirac nodal line net	DNL net	1	4	(11)	0	×	×	6 (2)	8 (4)
Nodal surface	NS	2	2	(1)	–	1257 (147)	×	765 (94)	×
Nodal surface net	NS net	2	2	(1)	–	442 (62)	×	168 (30)	×

types of emergent particles can exist in magnetic crystals with various MSGs.

Towards this goal, in this work we perform an exhaustive investigation of the emergent particles in type-III MSGs and compile an encyclopedia for them. This is done for each of the 674 type-III MSGs, and the lists of all possible emergent particles along with the symmetry conditions, the effective $\mathbf{k} \cdot \mathbf{p}$ Hamiltonians, and the topological characters of these particles for each type-III MSG is presented in Supplemental Material (SM) Sec. III [48]. The main results are summarized

in Tables I and II and the tables in SM Sec. I, corresponding to the list of all possible emergent particles in type-III MSGs and a quantitative mapping between the emergent particles and type-III MSGs, respectively. Our key findings are the following: (i) According to our classification, there exist a total 18 types of spinless emergent particles and 19 types of spinful emergent particles, as shown Table I. All these emergent particles can be realized in nonmagnetic systems. (ii) The type-III MSGs can also host several kinds of complex emergent particles, which are constituted by two different types of particles

TABLE II. Complex emergent particles existing in type-III MSGs. The format of this table is similar to Table I.

Notation	Abbr	d	Occurrence number			
			N_{ess}	N_{acc}	N_{ess}^{SOC}	N_{acc}^{SOC}
Combined WNL and NS	WNL/NS	2	68 (26)	×	54 (22)	×
Combined WNL net and NS net	WNLs/NSs	2	22 (9)	×	12(3)	×
Combined QNL and NS	QNL/NS	2	6(3)	×	6(3)	×
Combined QNL and WNL net	QNL/WNLs	2	166 (61)	×	×	×
Combined QNL net and WNL net	QNLs/WNLs	2	18 (18)	×	×	×

(see Table II). Remarkably, one of the complex quasiparticles, namely QNL/NS [combined quadratic nodal line (QNL) and nodal surface (NS)], only exists in magnetic systems. (iii) This encyclopedia provides a platform for systematic research on emergent particles by scanning all type-III MSGs. Compared with case-by-case study, the systematic research can usually provide comprehensive knowledge, complete inspection, and deep insights. Much important information can be inferred from our work. For example, with our classification, one knows that in type-III MSGs the largest topological charge (Chern number) for the nodal point is $|\mathcal{C}| = 3$ and the largest order of energy splitting for nodal line is quadratic. For comparison, the former is $|\mathcal{C}| = 4$ and the latter is cubic in type-II MSGs [5,49]. At last, for the complex particle QNL/NS, we also construct a concrete lattice model to demonstrate its existence and study its surface state.

Our work not only presents a complete classification and detailed analysis of the emergent particles in type-III MSGs but also is useful for searching novel topological magnetic materials with desired emergent particles. For example, for a given magnetic crystal, when the first-principles band structure are obtained, one can use our homemade `MSGcorep` package [50] to calculate the small corepresentations (coreps) of the degenerate bands. Then the species of the degeneracy can be directly identified by looking up the tables in this encyclopedia.

II. RATIONALE

The approach to obtain the results in this work is similar to that in Ref. [38]. We first calculate the small coreps at all high-symmetry k points and k lines in the Brillouin zone (BZ) of each of the 674 type-III MSGs based on our homemade package `SpaceGroupIrep` [51] and `MSGcorep` [50]. Both single-valued [for spinless systems, without spin-orbit coupling (SOC)] and double-valued coreps (for spinful systems, with SOC) are considered. Consider a type-III MSG M, which can be written as $M = S + \mathcal{T}(G - S)$ [52]. For a wave vector $\boldsymbol{k}$ in the BZ, its magnetic little group (MLG), denoted by $M_{\boldsymbol{k}}$, is the subgroup of M which is composed of the elements whose point parts leave $\boldsymbol{k}$ invariant, i.e., $M_{\boldsymbol{k}} = \{Q \mid Q \in M \& P(Q)\boldsymbol{k} \doteq \boldsymbol{k}\}$, in which $P(Q)$ means the point part of Q and $\doteq$ means two wave vectors differ by a reciprocal lattice vector. Note that $\mathcal{T}\boldsymbol{k} = -\boldsymbol{k}$, $P(Q) = R$ if $Q = \{R|\boldsymbol{t}\}$, and $P(Q) = \mathcal{T}R$ if $Q = \mathcal{T}\{R|\boldsymbol{t}\}$. The MLG $M_{\boldsymbol{k}}$ relates to the little group of $\boldsymbol{k}$ in S, denoted by $S_{\boldsymbol{k}}$, in two ways: (i) $M_{\boldsymbol{k}} = S_{\boldsymbol{k}}$, in this case there is no element $\{R|\boldsymbol{t}\}$ in $G - S$ which satisfies $R\boldsymbol{k} \doteq -\boldsymbol{k}$ and hence $M_{\boldsymbol{k}}$ is unitary; (ii) $M_{\boldsymbol{k}} = S_{\boldsymbol{k}} + A$, in this case $S_{\boldsymbol{k}}$ is the unitary subgroup of $M_{\boldsymbol{k}}$ and all elements in A are antiunitary with $|S_{\boldsymbol{k}}| = |A|$. Then the small coreps of $M_{\boldsymbol{k}}$ can be calculated according to the small representations of $S_{\boldsymbol{k}}$ [50–52]. Here, we adopt the convention used in the book [52] to describe MSG. The book uses the Belov-Neronova-Smirnova (BNS) notation [53,54] for MSG, but some MSGs are mistaken by the authors, which is also mentioned in [55]. We have corrected the MSGs which are not compatible with the BNS definition [50].

With the coreps information, we identify all the possible degeneracies including both essential and accidental degeneracies. For each degeneracy (at a certain high-symmetry

wave vector $\boldsymbol{k}_0$), we construct the $\boldsymbol{k} \cdot \boldsymbol{p}$ Hamiltonians according to the symmetry constraints

$$\begin{cases} \mathcal{D}(Q)H(\boldsymbol{k})\mathcal{D}(Q)^{-1} = H(R\boldsymbol{k}), & \text{if } Q = \{R|\boldsymbol{t}\} \\ \mathcal{D}(Q)H^*(\boldsymbol{k})\mathcal{D}(Q)^{-1} = H(-R\boldsymbol{k}), & \text{if } Q = \mathcal{T}\{R|\boldsymbol{t}\} \end{cases}, \quad (2)$$

where $\mathcal{D}(Q)$ is the unitary corep matrix of Q for each $Q \in M_{\boldsymbol{k}_0}$ and $\mathcal{D}(Q)$ can be either irreducible (for essential degeneracy) or reducible (for accidental degeneracy). Using the iteratively simplifying algorithm, $H(\boldsymbol{k})$ can be obtained up to any specified order of $\boldsymbol{k}$ [56]. Here we use the lowest order of $\boldsymbol{k}$ that is essential to make correct classification of emergent particles. Most of the physical properties of the degeneracies, such as energy dispersion and topological charge can be directly inferred from the constructed effective Hamiltonian. Finally, we classify all the band crossings by the standard of the classification established in [38] and the results are shown in Table I (refer to the SM of [38] for the details of each notation in Table I), Table II, and the tables in the SM [48]. It should be pointed out that Weyl points at general k points only need translation symmetries to protect them and hence they are not involved in our classification, as stated in [38].

In Table I, for each emergent particle, we explicitly list its occurrence number at the high-symmetry momenta of all type-III MSGs and also list the number of the type-III MSGs hosting it. For both counting numbers, four cases are listed separately: spinless essential particle, spinless accidental particle, spinful essential particle, and spinful accidental particle. These data can tell us which emergent particles are common and which ones are rare. The following points can be seen: (i) C-1 WP (charge-1 Weyl point) is very common and WP becomes more and more rare as $|\mathcal{C}|$ increases. Statistics further shows that C-2 WP only exists in tetragonal and hexagonal systems, and C-3 WP only exists on the $\Delta(00u)$ line in hexagonal systems. (ii) Accidental WP's are much more common than essential WP's, which is also true for TP (triple point), DP (Dirac point), and C-2 DP. (iii) CDP (cubic Dirac point), CCDP (cubic crossing Dirac point), and OP (octuple point) are very rare, especially since CDP only exists at the double-valued small corep $(A)A_7A_7$ of MSG 192.251 ($P6/m'c'c'$) (see Appendix A for the corep label). (iv) WNL (Weyl nodal line) is more common than C-1 WP, and WNL net is also very common.

Compared with the emergent particles in type-II MSGs [38], six types of emergent particles, i.e., C-4 WP, C-4 DP, C-4 QDP (charge-4 quadratic Dirac point), C-4 SP (charge-4 sextuple point), QCSP (quadratic contact sextuple point), and CNL (cubic nodal line) do not exist in type-III MSGs. Detailed differences are emphasized in red in Tables I and II, in which a red cross means the particle exists in type-II MSGs but not in type-III MSGs, a red number means the particle does not exist in type-II MSGs but exists in type-III MSGs, and a black number (cross) means the particle exists (does not exist) in both type-II and type-III MSGs. Consequently, one finds that all noncomplex particles in type-III MSGs also exist in type-II MSGs, and the complex emergent particle QNL/NS is the only one which exists in type-III MSGs but not in type-II MSGs.

TABLE III. Part of the spinless emergent particles in MSG 56.370 excerpted from the 56.370 tables in SM Secs. III A and III B. The first line indicates the information about the notation of MSG (its unitary subgroup in the parentheses), the Bravais lattice, the generators of the MSG, whether $I\mathcal{T}$ exists, and whether SOC is considered. $\boldsymbol{k}$ is a high-symmetry k point or k line defined in Table 3.6 of [52], "Generators" are the point parts for the generators of the MLG of $\boldsymbol{k}$, "Dim" is the dimension of the corep, and "matrices" are the corep matrices of the MLG generators. The unitary matrices λ_m, σ_p, and Γ_q are defined in SM Sec. IV. All $\boldsymbol{k} \cdot \boldsymbol{p}$ Hamiltonians are defined in SM Sec. V. Node type is just the type of emergent particles.

56.370, $Pc'cn'$ (14, $P2_1/c$) $\qquad\qquad\qquad\qquad$ Γ_o, $\{C_{2y}|\frac{1}{2}\frac{1}{2}0\}$, $\{I|\frac{1}{2}\frac{1}{2}\frac{1}{2}\}$, $\{C_{2x}\mathcal{T}|\frac{1}{2}\frac{1}{2}0\}$, without $I\mathcal{T}$, without SOC

k Name	k info	Generators	corep Label	corep Dim	corep matrices	$k \cdot p$ Hamiltonian	Node type	$|\mathcal{C}|$
Γ	000	$C_{2y}, I, C_{2x}\mathcal{T}$	$(\Gamma)\Gamma_1^+$	1	1,1,1	$H_{10.46}^{(\Gamma)\Gamma_1^+}$	–	
			$(\Gamma)\Gamma_1^-$	1	$1, -1, -1$	$H_{10.46}^{(\Gamma)\Gamma_1^-}$	–	
			$(\Gamma)\Gamma_2^+$	1	$-1, 1, -1$	$H_{10.46}^{(\Gamma)\Gamma_1^+}$	–	
			$(\Gamma)\Gamma_2^-$	1	$-1, -1, 1$	$H_{10.46}^{(\Gamma)\Gamma_1^+}$	–	
Y	$\bar{1}00$	$C_{2y}, I, C_{2x}\mathcal{T}$	$(Y)Z_1$	2	$\sigma_4, \sigma_3, \sigma_3$	$H_{50.282}^{(X)A_2}$	P-WNL	
U	$0\frac{1}{2}\frac{1}{2}$	$C_{2y}, I, C_{2x}\mathcal{T}$	$(U)A_1A_1$	4	$\Gamma_{49}, -\Gamma_{70}, -\Gamma_{10}$	$H_{56.370}^{(U)A_1A_1}$	DP	0
S	$\frac{1}{2}\frac{1}{2}0$	$C_{2y}, I, C_{2x}\mathcal{T}$	$(S)C_1$	2	$\sigma_4, \sigma_3, \sigma_4$	$H_{55.358}^{(X)B_2}$	P-NS	
R	$\bar{1}\frac{1}{2}\frac{1}{2}$	$C_{2y}, I, C_{2x}\mathcal{T}$	$(R)E_1^+E_2^+$	2	$i\sigma_3, -\sigma_0, -i\sigma_4$	$H_{55.358}^{(S)D_1^+D_2^+}$	P-WNL/NS	
			$(R)E_1^-E_2^-$	2	$i\sigma_3, \sigma_0, i\sigma_4$	$H_{55.358}^{(S)D_1^+D_2^+}$	P-WNL/NS	
D	XS	$C_{2y}, C_{2x}\mathcal{T}$	$(D)W_1W_2$	2	$\lambda_{20}\sigma_3, \lambda_{20}\sigma_4$	$H_{55.358}^{(D)V_1V_2}$	L-NS	
E	TR	$\sigma_y, C_{2z}\mathcal{T}$	$(E)UN_1UN_2$	2	$-i\sigma_3, \sigma_1$	$H_{27.80}^{(Z)B_1B_2}$	WNL	π
			Accidental degeneracy on high-symmetry k line					
Δ	ΓY	$C_{2y}, C_{2x}\mathcal{T}$	$\{(\Delta)\Lambda_1, (\Delta)\Lambda_2\}$	2	$\lambda_{20}\sigma_3, \lambda_{20}\sigma_3$	$H_{49.270}^{\{(\Delta)\Lambda_1, (\Delta)\Lambda_2\}}$	C-1 WP	1
Σ	ΓX	$\sigma_y, C_{2z}\mathcal{T}$	$\{(\Sigma)UN_1, (\Sigma)UN_2\}$	2	σ_3, σ_0	$H_{25.59}^{\{(\Sigma)UN_1, (\Sigma)UN_2\}}$	P-WNL	

III. AN EXAMPLE: MSG 56.370

As discussed above, we explore all the possibilities of the emergent particles in type-III MSGs and tabulate the results one MSG by MSG. The resulting tables are listed in the SM. We then use a spinless system with MSG no. 56.370 ($Pc'cn'$) as an example to provide a glimpse of the encyclopedia. Table III is an example excerpted from the tables for MSG 56.370 in SM Sec. III A and SM Sec. III B. In Table III, the first line provides some basic information of MSG 56.370, including unitary subgroup, BZ type, generating elements, whether the MSG has $I\mathcal{T}$ symmetry (combined spatial inversion symmetry I and $\mathcal{T}$), and whether SOC effect is considered.

The main part of Table III can be divided into six parts: information of high-symmetry momentum $\boldsymbol{k}$, the point parts of the generating elements of $M_{\boldsymbol{k}}$, the corep information of $M_{\boldsymbol{k}}$, and the effective Hamiltonian, the type and the topological charge of the degeneracies. Particularly, we find that many coreps share the same matrices and so do the $\boldsymbol{k} \cdot \boldsymbol{p}$ Hamiltonians. Thus, we also explicitly list all the possible corep matrices and Hamiltonians in SM Secs. IV and V respectively. For example, the corep matrices for the generators of $M_{\boldsymbol{k}=Y}$ are $\mathcal{D}(\{C_{2y}|\frac{1}{2}\frac{1}{2}0\}) = \sigma_4$ and $\mathcal{D}(\{I|\frac{1}{2}\frac{1}{2}\frac{1}{2}\}) = \mathcal{D}(\mathcal{T}\{C_{2x}|\frac{1}{2}\frac{1}{2}0\}) = \sigma_3$ [57] with

$$\sigma_4 = \begin{pmatrix} 0 & 1 \\ -1 & 0 \end{pmatrix}, \quad \sigma_3 = \begin{pmatrix} 1 & 0 \\ 0 & -1 \end{pmatrix},$$

and the effective Hamiltonian is

$$H_{50.282}^{(X)A_2} = c_2 k_x \sigma_1 - c_3 k_y \sigma_2 + c_1 \sigma_0.$$

The subscript and superscript in $H_{50.282}^{(X)A_2}$ means that this matrix form of effective Hamiltonian first appears for the degeneracy with corep $(X)A_2$ at MSG 50.282.

P-WNL (P-NS) indicates that the high-symmetry k point (e.g., Y, S) or the accidental band-crossing point on a high-symmetry k line (e.g., Σ) is actually a point residing on a WNL (NS), and similarly L-NS indicates that the high-symmetry k line (e.g., D) resides on a NS. Therefore, when counting the occurrence numbers in Tables I and II, P-WNL is regarded as WNL, P-WNL/NS is regarded as WNL/NS, and both P-NS and L-NS are regarded as NS.

IV. COMPLEX PARTICLE: QNL/NS

As mentioned above, QNL/NS is a novel complex emergent particle that does not exist in nonmagnetic systems. Here we take a spinful system hosting QNL/NS for example to demonstrate the existence of QNL/NS. There are three type-III MSGs hosting QNL/NS, i.e., 176.147 ($P6_3'/m'$), 193.259 ($P6_3'/m'cm'$), and 194.268 ($P6_3'/m'm'c$). Without loss of generality, we construct a tight-binding (TB) model under the symmetric constraints of MSG 176.147 by our homemade `MagneticTB` package [58]. The simplest s orbitals, i.e., $|s \uparrow\rangle$ and $|s \downarrow\rangle$, are adopted to construct the TB model, which is enough to capture QNL/NS. Figure 1(a) is the unit cell with irrelevant atoms omitted, showing an A-type antiferromagnetic configuration. The TB Hamiltonian is given in Appendix B.

The energy bands of the model are shown in Fig. 1(c), from which we can see that line Γ-A, line A-H (in fact the whole plane AHL), and point K are doubly degenerate. The four bands are divided into upper and lower portions which
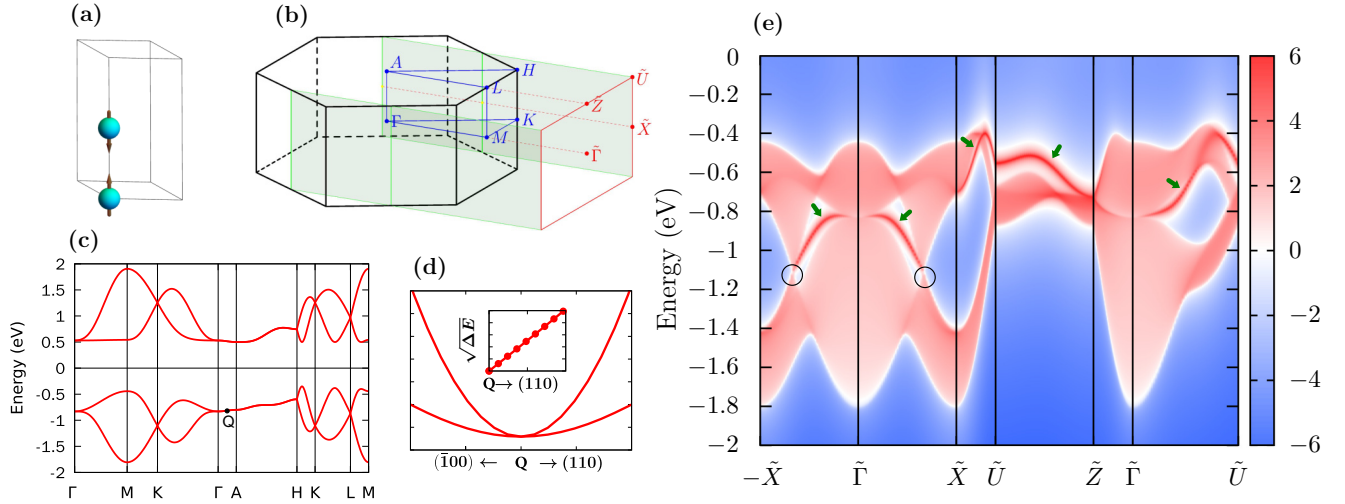
FIG. 1. Unit cell (a), bulk BZ and its projection to (100) surface (b), bulk energy bands (c),(d), and density of states of semi-infinite system with (100) surface (e) of the TB model of MSG 176.147. ΔE in (d) means the band splitting. The parameters used are $\varepsilon = -0.5$, $t_1 = 0.4$, $t_2 = -0.1$, $t_3 = 0$, $r = -0.8$, $s_1 = 0.2$, $s_2 = s_3 = s_4 = 0$.

are separated by a gap and possess the same degeneracy over the whole BZ. Accordingly, the lower two bands are enough to host all possible essential particles in MSG 176.147, including three noncomplex types, i.e., a QNL along Γ-A, a NS on plane AHL, and two C-1 WP's at $\pm K$ points, and a complex type QNL/NS at A point (cf. the 176.147 table in the SM Sec. III C). The band splitting around any point on Γ-A, such as the Q point in Fig. 1(c), is quadratic along both $(\bar{1}00)$ and (110) directions, as shown in Fig. 1(d), which indicates Γ-A is a QNL. Figure 1(e) shows the density of states of a semi-infinite system terminated by the (100) plane, in which the two circles indicate the projection of the two C-1 WP's at $\pm K$ onto the (100) surface BZ [see Fig. 1(b)] and the arrows indicate the surface states.

It should be pointed out that the coexistence of both QNL along Γ-A and NS on plane AHL does not necessarily lead to QNL/NS at the A point. The existence of QNL/NS requires that the coreps of QNL and NS satisfy the compatibility relation with the coreps of their intersection point. For example, the type-II MSG 176.144 ($P6_3/m1'$) have both QNL along Γ-A and NS on plane AHL but does not have QNL/NS at the A point [17,33]. None of type-II MSGs satisfies such compatibility relation and this is why QNL/NS does not exist in type-II MSGs.

V. CONCLUSIONS

In conclusion, we have studied all the possible emergent particles that can be stabilized by type-III MSG symmetries and compiled the results to an encyclopedia. Band crossings at all high-symmetry k points and k lines and originated from both single-valued and double-valued small coreps are analyzed. In addition to the essential degeneracy protected by a single small corep, accidental degeneracy induced by a pair of small coreps is also considered. Compared with the results of type-II MSGs in [38], the noncomplex emergent particles existing in type-III MSGs form a subset of those in type-II MSGs, missing C-4 WP, C-4 DP, C-4 QDP, C-4

SP, QCSP, and CNL in type-III MSGs. The complex particle QNL/NS is the only one which exists in type-III MSGs but not in type-II MSGs. One can easily check which type-III MSGs can host a certain emergent particle in SM Sec. I. Apart from the emergent particles, this encyclopedia provide a quick reference of all small coreps at/on every high-symmetry k point/k line defined in [52], and it also provides the $\boldsymbol{k} \cdot \boldsymbol{p}$ Hamiltonians for these k points/k lines. This work will be a convenient reference for emergent particles, symmetries, and $\boldsymbol{k} \cdot \boldsymbol{p}$ models in the study of magnetic topological nodal materials and related fields, and it will also facilitate the search for required emergent particles in magnetic materials.

APPENDIX A: LABEL OF SMALL COREP

The small corep of a type-III MSG $M = S + \mathcal{T}(G - S)$ is constructed from *one* or *two* of the small representations of its unitary subgroup S. The BZ and k point naming of M are the same as those of G, but they may be different from those of S. Taking MSG 118.309 ($P\bar{4}n'2$) for example, its S subgroup is space group no. 21 ($C222$). Hence M has a simple tetragonal BZ, while S has a base-centered orthogonal BZ. The k point

A for M corresponds to the k point T for S. Accordingly, we use the label $(A)T_1T_3$ to describe the small corep of the MLG $M_{\boldsymbol{k}(=A)}$ which is constructed from two small representations T_1 and T_3 of the little group $S_{\boldsymbol{k}(=T)}$. For the labels of small representations, such as the T_1 and T_3 here, the BC convention is adopted [51,52]. The symbol A in the parentheses explicitly indicates the k-point name for M, which is different from the k-point name T for S here. However, even if the k-point names for both M and S happen to be the same, we still keep the parentheses. For example, MSG 118.309 also has small coreps $(A)T_2$, $(V)H_1H_1$, $(\Lambda)\Lambda_1$, $(Z)Z_2Z_2$, $(R)R_1R_2$, and so on.

APPENDIX B: TB MODEL OF MSG 176.147

According to the symmetries in MSG 176.147, a TB model based on orbitals $\{|s\uparrow\rangle, |s\downarrow\rangle\}$ at each of the two magnetic atoms in the hexagonal cell shown in Fig. 1(a) can be constructed by the MagneticTB package [58] to show the existence of the QNL/NS emergent particle. The obtained Hamiltonian is

$$H(\boldsymbol{k}) = \begin{bmatrix} \varepsilon\sigma_3 + h_1 & h_2 + h_3 \\ h_2^+ + h_3^+ & \varepsilon\sigma_3 + h_1^* \end{bmatrix}, \tag{B1}$$

$$h_1 = \begin{bmatrix} t_2 f_1(\boldsymbol{k}_\parallel) & t_1 f_2(\boldsymbol{k}_\parallel) \\ t_1^* f_2^*(\boldsymbol{k}_\parallel) & t_3 f_1(\boldsymbol{k}_\parallel) \end{bmatrix}, \tag{B2}$$

$$h_2 = r\cos\frac{k_z}{2}\sigma_1, \tag{B3}$$

$$h_3 = \begin{bmatrix} s_3 f_2(\boldsymbol{k}_\parallel)\cos\frac{k_z}{2} & s_1 f_3(\boldsymbol{k}) + s_2 f_4(\boldsymbol{k}) \\ s_1 f_4(\boldsymbol{k}) + s_2 f_3(\boldsymbol{k}) & s_4 f_2^*(\boldsymbol{k}_\parallel)\cos\frac{k_z}{2} \end{bmatrix}, \tag{B4}$$

in which h_1, h_2, and h_3 are blocks from the first-, second-, and third-neighbour hoppings respectively, ε is a real parameter, and t_i, r, and s_j are complex hopping parameters (except t_2 and t_3 which are real). $\boldsymbol{k}_\parallel = (k_x, k_y)$, and f_i is defined as follows:

$$f_1(\boldsymbol{k}_\parallel) = \cos k_x + \cos k_y + \cos(k_x + k_y), \tag{B5}$$

$$f_2(\boldsymbol{k}_\parallel) = \cos k_x + e^{-i\frac{2\pi}{3}}\cos k_y + e^{-i\frac{4\pi}{3}}\cos(k_x + k_y), \tag{B6}$$

$$f_3(\boldsymbol{k}) = \cos\left(k_x - \frac{k_z}{2}\right) + \cos\left(k_y - \frac{k_z}{2}\right) \\ + \cos\left(k_x + k_y + \frac{k_z}{2}\right), \tag{B7}$$

$$f_4(\boldsymbol{k}) = \cos\left(k_x + \frac{k_z}{2}\right) + \cos\left(k_y + \frac{k_z}{2}\right) \\ + \cos\left(k_x + k_y - \frac{k_z}{2}\right). \tag{B8}$$

Compared with the original output of MagneticTB, in order to make the result tidy, we have adjusted the bases by the transformation matrix $\sigma_0 \oplus \sigma_1$ and substituted for the original parameters, i.e., $\varepsilon = (e2 - e1)/2$, $t_1 = 2[t1 + \frac{i}{\sqrt{3}}(t1 + 2t3)]$, $t_2 = 2t4$, $t_3 = 2t2$, $r = 2(r2 - ir1)$, $s_1 = 2(s5 + is1)$, $s_2 = 2(s8 + is2)$, $s_3 = 4[s6 + \frac{i}{\sqrt{3}}(2s3 + s6)]$, and $s_4 = 4[s7 - \frac{i}{\sqrt{3}}(2s4 + s7)]$.

[1] X. Wan, A. M. Turner, A. Vishwanath, and S. Y. Savrasov, Topological semimetal and fermi-arc surface states in the electronic structure of pyrochlore iridates, Phys. Rev. B **83**, 205101 (2011).

[2] S. M. Young, S. Zaheer, J. C. Y. Teo, C. L. Kane, E. J. Mele, and A. M. Rappe, Dirac Semimetal in Three Dimensions, Phys. Rev. Lett. **108**, 140405 (2012).

[3] A. A. Burkov, M. D. Hook, and L. Balents, Topological nodal semimetals, Phys. Rev. B **84**, 235126 (2011).

[4] Z. Wang, Y. Sun, X.-Q. Chen, C. Franchini, G. Xu, H. Weng, X. Dai, and Z. Fang, Dirac semimetal and topological phase transitions in A$_3$Bi (a=na, k, rb), Phys. Rev. B **85**, 195320 (2012).

[5] C. Fang, M. J. Gilbert, X. Dai, and B. A. Bernevig, Multi-Weyl Topological Semimetals Stabilized by Point Group Symmetry, Phys. Rev. Lett. **108**, 266802 (2012).

[6] A. A. Burkov and L. Balents, Weyl Semimetal in a Topological Insulator Multilayer, Phys. Rev. Lett. **107**, 127205 (2011).

[7] Z. K. Liu, B. Zhou, Y. Zhang, Z. J. Wang, H. M. Weng, D. Prabhakaran, S.-K. Mo, Z. X. Shen, Z. Fang, X. Dai, Z. Hussain, and Y. L. Chen, Discovery of a three-dimensional topological dirac semimetal, Na$_3$Bi, Science **343**, 864 (2014).

[8] S. M. Young and C. L. Kane, Dirac Semimetals in Two Dimensions, Phys. Rev. Lett. **115**, 126803 (2015).

[9] S.-Y. Xu, I. Belopolski, N. Alidoust, M. Neupane, G. Bian, C. Zhang, R. Sankar, G. Chang, Z. Yuan, C.-C. Lee, S.-M. Huang, H. Zheng, J. Ma, D. S. Sanchez, B. Wang, A. Bansil, F. Chou, P. P. Shibayev, H. Lin, S. Jia *et al.*, Discovery of a weyl fermion semimetal and topological fermi arcs, Science **349**, 613 (2015).

[10] A. A. Soluyanov, D. Gresch, Z. Wang, Q. Wu, M. Troyer, X. Dai, and B. A. Bernevig, Type-II Weyl Semimetals, Nature (London) **527**, 495 (2015).

[11] Z. Zhu, G. W. Winkler, Q. S. Wu, J. Li, and A. A. Soluyanov, Triple Point Topological Metals, Phys. Rev. X **6**, 031003 (2016).

[12] B. Bradlyn, J. Cano, Z. Wang, M. G. Vergniory, C. Felser, R. J. Cava, and B. A. Bernevig, Beyond dirac and weyl fermions: Unconventional quasiparticles in conventional crystals, Science **353**, aaf5037 (2016).

[13] C.-K. Chiu, J. C. Y. Teo, A. P. Schnyder, and S. Ryu, Classification of topological quantum matter with symmetries, Rev. Mod. Phys. **88**, 035005 (2016).

[14] N. P. Armitage, E. J. Mele, and A. Vishwanath, Weyl and dirac semimetals in three-dimensional solids, Rev. Mod. Phys. **90**, 015001 (2018).

[15] S. Li, Z.-M. Yu, Y. Liu, S. Guan, S.-S. Wang, X. Zhang, Y. Yao, and S. A. Yang, Type-II nodal loops: Theory and material realization, Phys. Rev. B **96**, 081106(R) (2017).

[16] Z. Yan, R. Bi, H. Shen, L. Lu, S.-C. Zhang, and Z. Wang, Nodal-link semimetals, Phys. Rev. B **96**, 041103(R) (2017).

[17] W. Wu, Y. Liu, S. Li, C. Zhong, Z.-M. Yu, X.-L. Sheng, Y. X. Zhao, and S. A. Yang, Nodal surface semimetals: Theory and material realization, Phys. Rev. B **97**, 115125 (2018).

[18] R. Bi, Z. Yan, L. Lu, and Z. Wang, Nodal-knot semimetals, Phys. Rev. B **96**, 201305(R) (2017).

[19] H. Weng, Y. Liang, Q. Xu, R. Yu, Z. Fang, X. Dai, and Y. Kawazoe, Topological node-line semimetal in three-dimensional graphene networks, Phys. Rev. B **92**, 045108 (2015).

[20] D.-S. Ma, J. Zhou, B. Fu, Z.-M. Yu, C.-C. Liu, and Y. Yao, Mirror protected multiple nodal line semimetals and material realization, Phys. Rev. B **98**, 201104(R) (2018).

[21] B. Fu, X. Fan, D. Ma, C.-C. Liu, and Y. Yao, Hourglasslike nodal net semimetal in Ag_2BiO_3, Phys. Rev. B **98**, 075146 (2018).

[22] M. Z. Hasan, G. Chang, I. Belopolski, G. Bian, S.-Y. Xu, and J.-X. Yin, Weyl, Dirac and high-fold chiral fermions in topological quantum matter, Nat. Rev. Mater. **6**, 784 (2021).

[23] X.-P. Li, K. Deng, B. Fu, Y. K. Li, D.-S. Ma, J. F. Han, J. Zhou, S. Zhou, and Y. Yao, Type-III Weyl semimetals: $(TaSe_4)_2I$, Phys. Rev. B **103**, L081402 (2021).

[24] Z. Wang, H. Weng, Q. Wu, X. Dai, and Z. Fang, Three-dimensional dirac semimetal and quantum transport in cd_3as_2, Phys. Rev. B **88**, 125427 (2013).

[25] H.-Z. Lu and S.-Q. Shen, Quantum transport in topological semimetals under magnetic fields, Front. Phys. **12**, 127201 (2017).

[26] D. T. Son and B. Z. Spivak, Chiral anomaly and classical negative magnetoresistance of weyl metals, Phys. Rev. B **88**, 104412 (2013).

[27] E. V. Gorbar, V. A. Miransky, and I. A. Shovkovy, Chiral anomaly, dimensional reduction, and magnetoresistivity of weyl and dirac semimetals, Phys. Rev. B **89**, 085126 (2014).

[28] T. Bzdušek, Q. Wu, A. Rüegg, M. Sigrist, and A. A. Soluyanov, Nodal-chain metals, Nature (London) **538**, 75 (2016).

[29] M. Ezawa, Loop-Nodal and Point-Nodal Semimetals in Three-Dimensional Honeycomb Lattices, Phys. Rev. Lett. **116**, 127202 (2016).

[30] G. Bian, T.-R. Chang, H. Zheng, S. Velury, S.-Y. Xu, T. Neupert, C.-K. Chiu, S.-M. Huang, D. S. Sanchez, I. Belopolski, N. Alidoust, P.-J. Chen, G. Chang, A. Bansil, H.-T. Jeng, H. Lin, and M. Z. Hasan, Drumhead surface states and topological nodal-line fermions in TlTaSe2, Phys. Rev. B **93**, 121113(R) (2016).

[31] B. J. Wieder, Y. Kim, A. M. Rappe, and C. L. Kane, Double Dirac Semimetals in Three Dimensions, Phys. Rev. Lett. **116**, 186402 (2016).

[32] Z.-M. Yu, Y. Yao, and S. A. Yang, Predicted Unusual Magnetoresponse in Type-II Weyl Semimetals, Phys. Rev. Lett. **117**, 077202 (2016).

[33] Z.-M. Yu, W. Wu, X.-L. Sheng, Y. X. Zhao, and S. A. Yang, Quadratic and cubic nodal lines stabilized by crystalline symmetry, Phys. Rev. B **99**, 121106(R) (2019).

[34] T. Bzdušek and M. Sigrist, Robust doubly charged nodal lines and nodal surfaces in centrosymmetric systems, Phys. Rev. B **96**, 155105 (2017).

[35] R. Yu, Z. Fang, X. Dai, and H. Weng, Topological nodal line semimetals predicted from first-principles calculations, Front. Phys. **12**, 127202 (2017).

[36] W. Chen, H.-Z. Lu, and O. Zilberberg, Weak Localization and Antilocalization in Nodal-Line Semimetals: Dimensionality and Topological Effects, Phys. Rev. Lett. **122**, 196603 (2019).

[37] N. Nagaosa, T. Morimoto, and Y. Tokura, Transport, magnetic and optical properties of weyl materials, Nat. Rev. Mater. **5**, 621 (2020).

[38] Z.-M. Yu, Z. Zhang, G.-B. Liu, W. Wu, X.-P. Li, R.-W. Zhang, S. A. Yang, and Y. Yao, Encyclopedia of emergent particles in three-dimensional crystals, Sci. Bull. (2022), doi: 10.1016/j.scib.2021.10.023.

[39] P. Tang, Q. Zhou, G. Xu, and S.-C. Zhang, Dirac fermions in an antiferromagnetic semimetal, Nat. Phys. **12**, 1100 (2016).

[40] Q. Wang, Y. Xu, R. Lou, Z. Liu, M. Li, Y. Huang, D. Shen, H. Weng, S. Wang, and H. Lei, Large intrinsic anomalous Hall effect in half-metallic ferromagnet $Co_3Sn_2S_2$ with magnetic Weyl fermions, Nat. Commun. **9**, 3681 (2018).

[41] Q. Xu, E. Liu, W. Shi, L. Muechler, J. Gayles, C. Felser, and Y. Sun, Topological surface Fermi arcs in the magnetic Weyl semimetal $Co_3Sn_2S_2$, Phys. Rev. B **97**, 235416 (2018).

[42] D. F. Liu, A. J. Liang, E. K. Liu, Q. N. Xu, Y. W. Li, C. Chen, D. Pei, W. J. Shi, S. K. Mo, P. Dudin, T. Kim, C. Cacho, G. Li, Y. Sun, L. X. Yang, Z. K. Liu, S. S. P. Parkin, C. Felser, and Y. L. Chen, Magnetic Weyl semimetal phase in a Kagomé crystal, Science **365**, 1282 (2019).

[43] N. Morali, R. Batabyal, P. K. Nag, E. Liu, Q. Xu, Y. Sun, B. Yan, C. Felser, N. Avraham, and H. Beidenkopf, Fermi-arc diversity on surface terminations of the magnetic Weyl semimetal $Co_3Sn_2S_2$, Science **365**, 1286 (2019).

[44] S. Nie, Y. Sun, F. B. Prinz, Z. Wang, H. Weng, Z. Fang, and X. Dai, Magnetic Semimetals and Quantized Anomalous Hall Effect in EuB_6, Phys. Rev. Lett. **124**, 076403 (2020).

[45] J. Wang, Antiferromagnetic topological nodal line semimetals, Phys. Rev. B **96**, 081107(R) (2017).

[46] B. Wang, H. Gao, Q. Lu, W. Xie, Y. Ge, Y.-H. Zhao, K. Zhang, and Y. Liu, Type-I and type-II nodal lines coexistence in the antiferromagnetic monolayer $CrAs_2$, Phys. Rev. B **98**, 115164 (2018).

[47] Z. Zhang, Z.-M. Yu, and S. A. Yang, Magnetic higher-order nodal lines, Phys. Rev. B **103**, 115112 (2021).

[48] See Supplemental Material at http://link.aps.org/supplemental/10.1103/PhysRevB.105.085117 for detailed tables of the emergent particles at/on each high-symmetry k point/k line for each of the 674 type-III MSGs.

[49] C. Cui, X.-P. Li, D.-S. Ma, Z.-M. Yu, and Y. Yao, Charge-four Weyl point: Minimum lattice model and chirality-dependent properties, Phys. Rev. B **104**, 075115 (2021).

[50] G.-B. Liu, Z. Zhang, Z.-M. Yu, and Y. Yao, `MSGcorep`: A package for corepresentations of magnetic space groups (unpublished).

[51] G.-B. Liu, M. Chu, Z. Zhang, Z.-M. Yu, and Y. Yao, `SpaceGroupIrep`: A package for irreducible representations of space group, Comput. Phys. Commun. **265**, 107993 (2021).

[52] C. J. Bradley and A. P. Cracknell, *The mathematical theory of symmetry in solids—representation theory for point groups and space groups* (Oxford University Press, New York, 2009).

[53] N. V. Belov, N. N. Neronova, and T. S. Smirnova, 1651 shubnikov groups, Sov. Phys. Crystallogr. **1**, 487 (1957).

[54] N. V. Belov, N. N. Neronova, and T. S. Smirnova, Shubnikov groups, Sov. Phys. Crystallogr. **2**, 311 (1957).

[55] F. Tang and X. Wan, Exhaustive constructions of effective models in 1651 magnetic space groups, Phys. Rev. B **104**, 085137 (2021).

[56] Z. Zhang, G.-B. Liu, Z.-M. Yu, and Y. Yao, MagneticKP: A package for $k \cdot p$ model of magnetic and non-magnetic materials (unpublished).

[57] The commands `getMLGElem[{56,370},"Y"]` and `showMLGCorep[{56,370},"Y"]` in the package `MSGcorep`

[50] can easily give respectively the elements and coreps of this MLG.

[58] Z. Zhang, Z.-M. Yu, G.-B. Liu, and Y. Yao, MagneticTB: A package for tight-binding model of magnetic and non-magnetic materials, Comput. Phys. Commun. **270**, 108153 (2022).